Lab 4: Nuclear Reactions and Nucleosynthesis

Otho Ulrich, Eugene Kopf, Mike Pirkola, Jacob Burke, Andrew Messecar, Spencer Henning, Asghar Kay

March 27, 2017

Abstract

A 2 MeV proton beam is used to annihilate lithium and flourine atoms from a LiF foil, transforming them to helium and oxygen through the nuclear reactions ^{19}F(p,α)^{16}O and ^{7}Li(p,α)^{4}He. Alpha particle detection is used to verify the nuclear reactions involved. Rutherford scattering of a proton against silicon and copper atoms is used to calibrate a kinetic energy scale to the channels of the MCA, but some problems with this are indicated by an imprecise fitting to the nuclear reaction peaks. The nuclear reaction peaks are nonetheless identified and their differential cross-section ratios are computed and compared positively with known values. Absolute cross-sections are also computed, but are dubious due to an unknown foil thickness.

1 Introduction: Lithium and Fluorine

The nuclear properties of lithium are of interest, especially the reaction differential cross-section for ^{7}Li(p,α)^{4}He. Studies of the Sun's photosphere show the abundance of lithium relative to hydrogen and helium less nearly an order of magnitude. A large cross-section for ^{7}Li(p,α)^{4}He is believed responsible; it predicts that ionized hydrogen will readily collide with lithium, transforming the lithium to helium, and emitting an alpha particle. This is one transition that takes place in stellar nucleosynthesis, and is maintained as fresh lithium is carried toward a star's core by convective currents, but even with this process and reaction in mind, modern astrophysicists have yet to completely explain the lack of abundant lithium in our sun's photosphere. Studies of the nuclear properties of lithium could elucidate a better stellar structure model, but this is outside the scope of our study. [2]

Fluorine can be rearranged in a similar fashion. It is one of the rarest elements observed by astronomers, and thought to be for the same reasons: it is readily rearranged by a proton to produce oxygen and an alpha particle. Figure 1 shows relative abundances of many elements. To judge whether the high-probability explanation is plausible, we will determine the reaction differential cross-sections of the fluorine-proton reaction ^{19}F(p,α)^{16}O and the lithium-proton reaction ^{7}Li(p,α)^{4}He. In this study, we performed a prompt radiation analysis by observing the alpha particle products of each reaction, and from the kinetic energy spectrum of these products, the differential cross-sections are computed.

2 Proton Beam and Detector

The Tandem Van de Graff Accelerator Lab provided a 1.95 ± 0.05 MeV proton beam for three experiments. When incident on a lithium-fluoride foil, we expect the nuclear reactions described in Section 3 to occur. When the beam is incident on a silicon or copper foil, we expect Rutherford

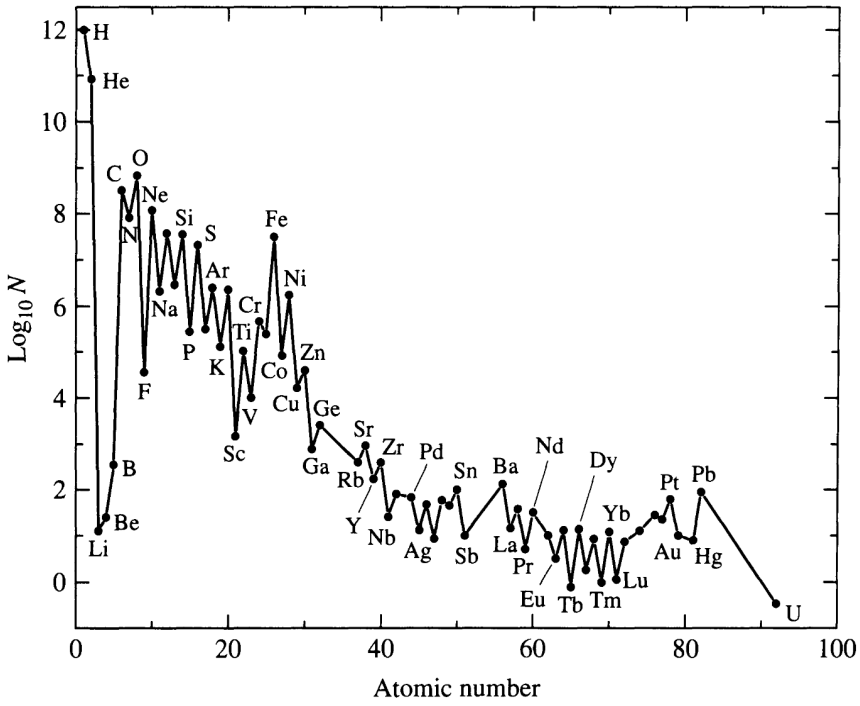

Figure 1: Relative elemental abundances in the sun's photosphere. Lithium and fluorine are much less abundant than their neighbor elements. It is thought this is due to large reaction differential cross-sections for a proton collision with these nuclei. [2]

scattering. We used a circular normal-faced surface barrier detector to observe the alpha particle products of ^{19}F(p,α)^{16}O and ^{7}Li(p,α)^{4}He and the protons from Rutherford scattering. [7] The detector was positioned at $149.95^\circ \pm 0.05^\circ$ from the proton beam, which we define as the lab frame of reference; see figure 2. The detector covers a solid angle $\Omega = 1.895 \pm 0.001$ steradians. In each experiment, the beam is run until total integrated charged reaches 2.00000×10^{-4} coulombs, corresponding to a total number of incident beam particles n = 1.24830×10^{15} protons.

The measurement apparatus serves to create a kinetic energy spectrum of charged particles. An alpha particle or proton (or any other charged particle) incident on the detector creates a current pulse which is converted to a voltage pulse across a high-impendence conductor. The voltage signal is then sent by way of a pre-amplifier to the receiving amplifier in the control room. A multi-channel analyzer receives voltage signals from the second amplifier, binning counts as a function of voltage. The amplifier is adjustable, allowing the voltage range to fit properly within the MCA's detection domain, and the voltage received at the MCA is directly proportional to the kinetic energy of the alpha particle. [7] In Section 3.1, a kinetic energy scale is calibrated to the voltage scale, thus providing the charged-particle spectrum.

3 Nuclear Reactions and Detection Plan

The nuclear reactions ^{19}F(p,α)^{16}O and ^{7}Li(p,α)^{4}He can be analyzed in terms of the kinematic diagram in figure 3. In this diagram, each M#,E# pair refers to the mass and kinetic energy of a particle involved in the collision, with associations defined in table 1. In the case where the incident particle does not have sufficient kinetic energy to overcome the electric potential barrier of the target nucleus, Rutherford scattering will occur. When it does overcome the potential barrier,

Figure 2: The detector was positioned at $149.95° \pm 0.05°$ relative to the direction of the proton beam. This angle was maintained through both experiments.

M1,E1:	Incident Particle
M2,E2:	Target Nucleus
M3,E3:	Emitted Particle
M4,E4:	Residual Nucleus

Table 1: These variables represent the mass and kinetic energies of the particles involved in the collision described in figure 3.

a nuclear reaction may occur. We ignore tunneling in this analysis, which is a potential source of error.

3.1 Calibration with Rutherford Scattering

The maximum expected kinetic energy resulting in Rutherford scattering can be computed, and by observing this value, the energy scale of the detector can be calibrated. Rutherford scattering can be analyzed in terms of figure 3, where M1 = M3, and M2 = M4. The scattering angle $\theta = 149.95° \pm 0.05°$. When we assume the collision is elastic, the kinetic energy of the scattered Proton $E3 \propto E1$. We define a kinematic factor K as the constant of proportionality. This factor can be computed as [7]

$$K = \left(\frac{M1cos(\theta) + \left(M2^2 - M1^2 sin^2(\theta)\right)^{1/2}}{M1 + M2} \right)^2 . \tag{1}$$

Thus,

$$E3 = K \times E1. \tag{2}$$

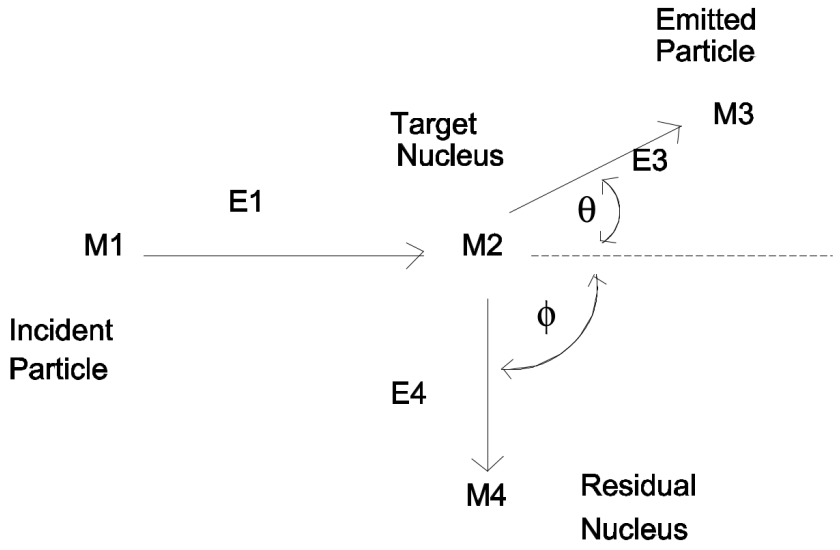

Figure 3: In general, an incident particle collides with a target nucleus, resulting in an emitted particle and a residual nucleus. In our experiments, the detection angle $\theta = 149.95° \pm 0.05°$ [7].

Isotope	Mass (amu)	Abundance	Kinematic Factor	
p/^{1}H^{+}	1.00727646688(13)			[2]
α/^{4}He^{++}	4.001506179127(63)			[6]
^{4}He	4.002603	1.000		[3]
^{7}Li	7.016004			[3]
^{16}O	15.994915	0.9976		[3]
^{19}F	18.998405			[3]
^{28}Si	28.086	1.0000	0.8746	[8]
^{63}Cu	62.930	0.6917	0.9420	[8]
^{65}Cu	64.928	0.3083	0.9437	[8]

Table 2: Properties of nuclei and particles important in our reactions. Li and F nuclei are constituent to LiF foil and are expected to undergo nuclear reactions, with residual nuclei ^{16}O and ^{4}He. The Cu and Si nuclei are involved in Rutherford scattering. p and α refer to a proton and an alpha particle, respectively. Abundances are relative to unit probability for that species, and kinematic factors are included for target nuclei involved in Rutherford scattering of a proton at 150°. Numbers reported without uncertainty are assumed to have uncertainty ± 1 on the most precise digit.

Reaction	Energy (MeV) Computed	Pub.	Dev.
^{28}Si(p)	1.706±0.05		
^{63}Cu(p)	1.837±0.05		
^{65}Cu(p)	1.840±0.05		
^{19}F(p,α)^{16}O	7.949±0.03	6.9	1.049(15%)
^{7}Li(p,α)^{4}He	7.688±0.03	7.7	0.012(0.2%)

Table 3: Expected kinetic energies for nuclear reactions and maximum energy of a Rutherford scattered proton. Rutherford scattering energies are computed using equation 2 with the kinematic factors from table 2. The expected alpha particle energy for ^{7}Li(p,α)^{4}He is in good agreement with that published in Chu et al., but the expectation for ^{19}F(p,α)^{16}O deviates by 15%. [3]

We observe Rutherford scattering of a proton by copper and silicon atoms by performing two experiments, one where the proton beam is incident on a copper foil, and then a silicon foil. Kinematic factors are tabulated in table 2. The proton may deposit energy in the target material, so the elastic case is the maximum energy case. A spectrum of energy from scattered protons should therefore be observed, a sum of approximately Gaussian peaks that drops to noise after this highest-energy peak. The expected peaks are tabulated in table 3.

3.2 Nuclear Reaction Peaks

The kinetic energy of the alpha particle products from ^{19}F(p,α)^{16}O and ^{7}Li(p,α)^{4}He are characteristic of those reactions. Binding energies of the involved nuclei are significant compared to their rest masses, so the relativistic equivalence must be considered when computing the energy Q released or absorbed during the reaction, [7] so

$$Q = \delta(mc^2) = (M1 + M2)c^2 - (M3 + M4)c^2. \tag{3}$$

After computing Q this way, non-relativistic conservations of total energy and momentum provide a sufficiently useful expression for the kinetic energy of the alpha particle product E3 as a function of the kinematic quantities described in figure 3. [9] With results in table 3, the expectation values of E3 were computed as [5]

$$E3^{1/2} = A \pm (A^2 + B)^{1/2}, \tag{4}$$

where

$$A = [(M1{\times}M3{\times}E1)^{1/2}/(M3 + M4)]cos\theta \tag{5}$$

and

$$B = [M4{\times}Q + E1(M4 - M1)]/(M3 + M4). \tag{6}$$

4 Results

The Rutherford scattering curves used to calibrate the energy scale are shown in figures 4 and 5. The best fit for this linear scale is

$$x = 0.009 \text{ MeV} \times \text{channel} + 0.00392 \text{ MeV}. \tag{7}$$

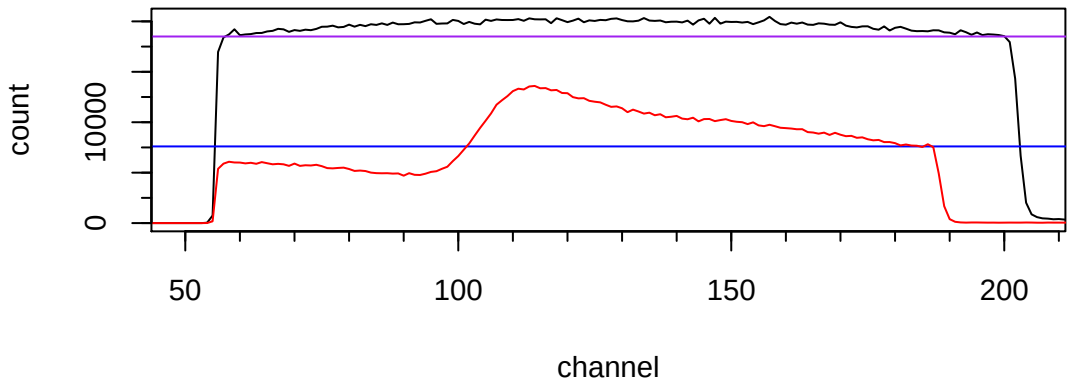

Figure 4: Across channels 50 through 205, we observed the signal from Rutherford scattering of protons by copper nuclei (black) and silicon nuclei (red). The maximum count before the cutoff is estimated at 7600 and 18500 and drawn with the blue and purple line, respectively.

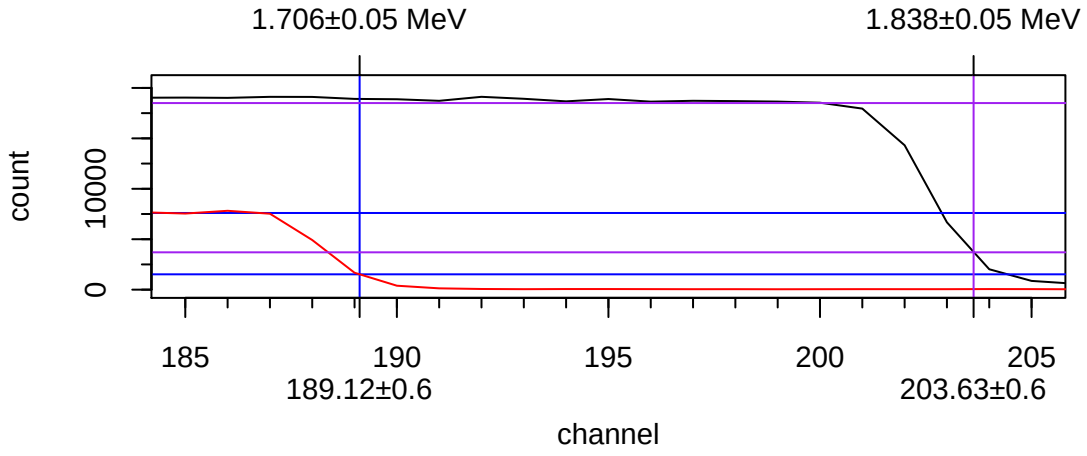

Figure 5: The kinetic energy scale is calibrated to channel number using the Rutherford energies predicted in table 3. The scale is set where the predicted energy matches 20% of the maximum before cutoff. The 20% line is drawn in the same color as its associated maximum line, and same for the identified energy coordinate.

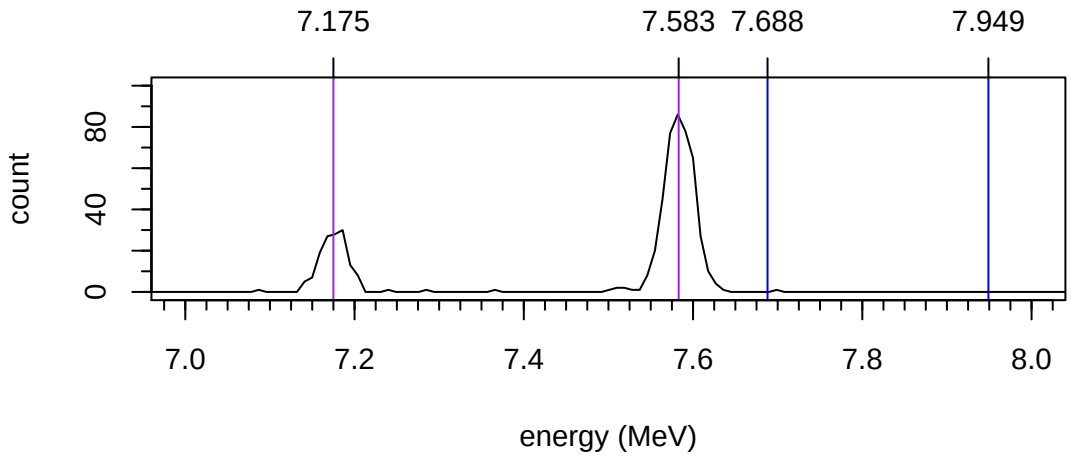

Figure 6: Two peaks were observed not far from the predicted energies along the calibrated scale. The peaks do not match the computed expected values (blue), but we progress under the assumption that the scale is wrong and the peaks identified (purple) are in fact the alpha particles predicted as products of the ^{7}Li(p,α)^{4}He and ^{19}F(p,α)^{16}O reactions.

An attempt is made to locate the predicted peaks for the alpha particle products of ^{7}Li(p,α)^{4}He and ^{19}F(p,α)^{16}O in figure 6. Two peaks are visible, but not at the predicted energies under our calibration. Presuming our calibration is off, the counts under these peaks are integrated to be used in computing the differential cross-section.

4.1 Yield and Differential Cross-Sections

We observed the reaction yield Y(θ) as the total count integrated under the curve for each reaction. Computing the differential cross-section for a reaction is done using [9]

$$\sigma(\theta, E) = Y(\theta, E)/(nN\delta x\Omega), \tag{8}$$

where

θ	=	detector angle,
E	=	energy referring to a specific reaction,
n	=	number of incident beam particles,
N	=	volume number density of target atoms,
δx	=	target thickness,
Ω	=	detector solid angle.

Beam and detector parameters can be referenced from section 2. The number densities for Li and F in an LiF foil are N(Li) = N(F) = 6.16 $\times 10^{22}$ atoms/cm^3. [1] However, the foil thickness is not known. Our best guess is 200$\pm$20 Å, but not knowing this thickness may dictate we only compute the ratio of the cross-sections rather than their absolute values. From equation 8,

$$\frac{\sigma(E_1)}{\sigma(E_2)} = \frac{Y(E_1)}{Y(E_2)}. \tag{9}$$

Reaction	Yield	Ratio	σ (cm^2)	σ (barns)
^{7}Li(p,α)^{4}He	428	3.12	(1.48±0.15)×10^{-38}	(1.48±0.15)×10^{-}14
^{19}F(p,α)^{16}O	137	0.320	(0.475±0.047)×10^{-38}	(0.475±0.047)×10^{-}14

Table 4: Yields and differential cross-sections computed for the reactions of interest. The ratio of each reaction's cross-section to the other is tabulated. The cross-section is computed using a foil thickness of 200±20Å, but this is only a guess.

4.2 Foil Thickness

The foil thickness δx is not known a priori but it may be determined using the Rutherford scattering of the alpha particle product from ^{19}F(p,α)^{16}O. The film thickness is less than 1000 Å, so it can be computed using the surface energy approximation as [4]

$$\delta x = \delta E1\{K[dE/dx]_{E1} + |cos\theta|^{-1}[dE/dx]_{KE1}\}^{-1}. \quad (10)$$

Here, δ E1 is the full width at half maximum of the Rutherford-scattered peak given a film thickness δ x. The stopping power terms [dE/dx] are referenced from appendix F of Chu et al., [3] where E1 refers to the incident alpha particle (the product of the ^{19}F(p,α)^{16}O reaction), and KE1 refers to the Rutherford-scattered alpha particle. The table of stopping cross sections consulted [3] did not provide values for the known alpha particle energy from this reaction, so an attempt was made to compute the value using the polynomial fit provided in table VII of that text. The output from this attempt was nonsense, so while this is a viable method for computing the foil thickness, thus allowing a better computation of the differential cross-sections of both reactions, the task of computing the foil thickness is not completed here.

5 Conclusion

The energy scale may be mis-calibrated due to a poor choice in locating the Rutherford scattering energy along the curve, however, looking at the difference between selecting the 100% mark rather than the 20% reveals a scale shift of only .018 MeV, less than 10% of the scale's deviation from the observed nuclear reaction peaks. This indicates a more significant flaw in the analysis remains to be uncovered. However, the peaks in the kinetic energy spectrum related to ^{19}F(p,α)^{16}O and ^{7}Li(p,α)^{4}He were identified near 7.175 MeV and 7.583 MeV respectively, and counts were taken by integrating under those features.

The ratio of the counts was used to compute the ratio of the differential cross-sections between these reactions, as in equation 9. For ^{19}F(p,α)^{16}O relative to ^{7}Li(p,α)^{4}He the ratio is 0.320. Chu et al. report yields for ^{19}F(p,α)^{16}O and ^{7}Li(p,α)^{4}He at 3 counts/μC and 9 counts/μC respectively [3], giving a ratio of 1/3. Our result deviates by 4%, indicating a strong agreement with published values.

Absolute values for the differential cross-sections of each reaction are computed in cm^2 and in barns, but these rely on a guess for the LiF foil thickness. An attempt was made to compute the foil thickness, but it ended in no useful values. With further work, this computation may be possible using only the information contained in this study. Without a value, the absolute differential cross-sections have little meaning, and can't inform the availability of these processes for stellar nuclear processes. However, it is clear that there is at least some significant availability, which could be sufficient in the proton-rich environment of stellar plasmas.

References

[1] N.W. Ashcroft and N.D. Mermin. *Solid state physics*. Science: Physics. Saunders College, 1976. ISBN: 9780030493461. URL: https://books.google.com/books?id=FRZRAAAAMAAJ.

[2] Bradley W. Carroll and Dale A. Ostlie. *An Introduction to Modern Astrophysics*. 2nd ed. pp. 542. 1301 Sansome St., San Fransisco, CA 94111: Pearson Education, Inc., publishing as Addison-Wesley, 2007. ISBN: 0-321-44284-9.

[3] Wei-Kan Chu, James W. Mayer, and Marc-A. Nicolet. *Backscattering Spectrometry*. 1st ed. pp 213. 111 Fifth Avenue, New York, New York 10003: Academic Press, 1978. ISBN: 0-12-173850-7.

[4] Leonard C. Feldman. *Fundamentals of Surface Thin Film Analysis*. Prentice Hall PTR, Aug. 1986. ISBN: 9780135005705.

[5] W. Meisel. "Surface and Thin Film Analysis by Mössbauer Spectroscopy and Related Techniques". In: *Mössbauer Spectroscopy Applied to Magnetism and Materials Science*. Ed. by Gary J. Long and Fernande Grandjean. Boston, MA: Springer US, 1996, pp. 1–30. ISBN: 978-1-4899-1763-8. DOI: 10.1007/978-1-4899-1763-8_1. URL: http://dx.doi.org/10.1007/978-1-4899-1763-8_1.

[6] Peter J. Mohr, Barry N. Taylor, and David B. Newell. *CODATA recommended values of the fundamental physical constants: Alpha Particle Mass in u*. June 2015. URL: http://physics.nist.gov/cgi-bin/cuu/Value?malu.

[7] Richard H. Schaus et al. *Nuclear Reactions*. Lab Guide. Montana State University, Western Michigan University, Mar. 2016.

[8] J.R. Tesmer and M.A. Nastasi. *Handbook of modern ion beam materials analysis*. Mrs Symposium Proceedings Series. Materials Research Society, 1995. ISBN: 9781558992542. URL: https://books.google.com/books?id=-YJUAAAAMAAJ.

[9] J.F. Ziegler. *New uses of ion accelerators*. Plenum Press,New York, Jan. 1975.